Superresolving Imaging of Arbitrary One-Dimensional Arrays of Thermal Light Sources Using Multiphoton Interference

Anton Classen,[1,2,*] Felix Waldmann,[1] Sebastian Giebel,[1] Raimund Schneider,[1,2] Daniel Bhatti,[1,2] Thomas Mehringer,[1,2] and Joachim von Zanthier[1,2]

[1]*Institut für Optik, Information und Photonik, Universität Erlangen-Nürnberg, 91058 Erlangen, Germany*

[2]*Erlangen Graduate School in Advanced Optical Technologies (SAOT), Universität Erlangen-Nürnberg, 91052 Erlangen, Germany*

(Received 29 July 2016; published 15 December 2016)

We propose to use multiphoton interferences of photons emitted from statistically independent thermal light sources in combination with linear optical detection techniques to reconstruct, i.e., image, arbitrary source geometries in one dimension with subclassical resolution. The scheme is an extension of earlier work [S. Oppel *et al.*, Phys. Rev. Lett. **109**, 233603 (2012)], where N regularly spaced sources in one dimension were imaged by use of the Nth-order intensity correlation function. Here, we generalize the scheme to reconstruct any number of independent thermal light sources at arbitrary separations in one dimension, exploiting intensity correlation functions of order $m \geq 3$. We present experimental results confirming the imaging protocol and provide a rigorous mathematical proof for the obtained subclassical resolution.

DOI: 10.1103/PhysRevLett.117.253601

Higher order interferences with photons emitted by statistically independent light sources are an active field of research with the potential to increase the resolution in spectroscopy, lithography, and interferometry [1–6], as well as in imaging and microscopy [7–20]. So far, subclassical resolution has been achieved by using entangled photons [3,8], but it was also shown that initially uncorrelated light fields—nonclassical as well as classical—can be employed for that purpose [13–20]. Recently, Oppel *et al.* presented a detection scheme that allows us to determine the source distance d for an array of N equidistant thermal light sources (TLS) with subclassical resolution by measuring the Nth-order spatial intensity correlation function [14].

In this Letter we show that the scheme presented in Ref. [14] can be generalized to reconstruct, i.e., image, any number of independent TLS at arbitrary separations in one dimension, by exploiting photon correlation functions of order $m \geq 3$. Measuring higher order correlations enables us to isolate the spatial frequencies of the setup allowing us to determine the source distribution with a resolution below the classical Abbe limit. We outline the imaging protocol and present experimental results verifying the theoretical predictions. A physical explanation and rigorous mathematical proof of the protocol and the spatial frequency filtering process is given in the Supplemental Material [21].

We assume N TLS aligned on a grid in one dimension with lattice constant d at arbitrary separations, such that $|\mathbf{R}_{l+1} - \mathbf{R}_l| = x_l d$, with $x_l \in \mathbb{N}$, $l = 1, \ldots, N-1$. The source geometry is thus determined by the lattice constant d and the $N-1$ adjacent source distances $\mathbf{x} = (x_1, x_2, \ldots, x_{N-1})$, whereas the spatial frequencies of the system are given by the tuple of source pair distances $\{\xi\} \equiv \{(x_1); (x_1 + x_2); \ldots; (x_{l_1} + \cdots + x_{l_2}); \ldots; (x_1 + \cdots + x_{N-1})\}$ (see Fig. 1).

To access the set of spatial frequencies $\{\xi\}$ we make use of the normalized spatial mth-order intensity correlation function $g_N^{(m)}(\mathbf{r}_1, \ldots, \mathbf{r}_m)$ obtained by correlating the intensities at positions $\mathbf{r}_1, \ldots, \mathbf{r}_m$ in the far field [31],

$$g_N^{(m)}(\mathbf{r}_1, \ldots, \mathbf{r}_m) \equiv \frac{\langle : \prod_{j=1}^{m} \hat{E}^{(-)}(\mathbf{r}_j) \hat{E}^{(+)}(\mathbf{r}_j) : \rangle_\rho}{\prod_{j=1}^{m} \langle \hat{E}^{(-)}(\mathbf{r}_j) \hat{E}^{(+)}(\mathbf{r}_j) \rangle_\rho}. \quad (1)$$

Here, $\langle : \cdot \cdot : \rangle_\rho$ denotes the (normally ordered) quantum mechanical expectation value for a system in the state ρ and $\hat{E}^{(-)}(\mathbf{r}_j)$ and $\hat{E}^{(+)}(\mathbf{r}_j)$ are the positive and negative frequency parts of the total electric field operator at position $\mathbf{r}_j$, given by $\hat{E}^{(+)}(\mathbf{r}_j) = [\hat{E}^{(-)}(\mathbf{r}_j)]^\dagger \propto \sum_l e^{ikr_{lj}} \hat{a}_l$ [14]. In the last expression, $\hat{a}_l$ is the annihilation operator of a photon emitted by source l at $\mathbf{R}_l$ and $r_{lj} = |\mathbf{R}_l - \mathbf{r}_j|$. Note that since we assume the emitters to be statistically independent, the state of the field is given by $\rho = \otimes_l \rho_l$,

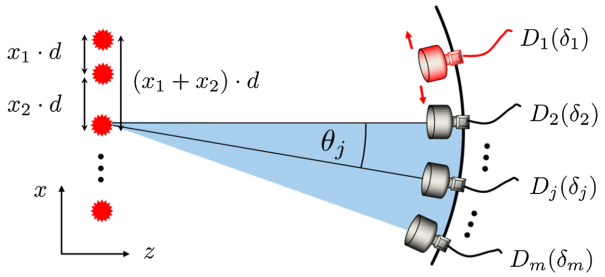

FIG. 1. Scheme of the considered setup: N TLS are arbitrarily aligned on a grid in one dimension with lattice constant d such that $|\mathbf{R}_{l+1} - \mathbf{R}_l| = x_l d$, with $x_l \in \mathbb{N}$, $l = 1, \ldots, N-1$. In the far field of the sources m detectors D_j, $j = 1, \ldots, m$, measure the intensities at $\mathbf{r}_1, \ldots, \mathbf{r}_m$, with $\delta_j = \delta_j(\mathbf{r}_j) = kd \sin[\theta_j(\mathbf{r}_j)]$.

with $\rho_l = \sum_n P_l(n)|n\rangle\langle n|$, where $P_l(n)$ is the photon number distribution of source l [32].

In the case of a regular source arrangement with N equidistant TLS at separation d and $m-1$ detectors placed at $\mathbf{r}_2 = \cdots = \mathbf{r}_m = 0$ the mth-order correlation function as a function of the position of the first detector takes the form $g_N^{(m)}(\mathbf{r}_1;0) \equiv g_N^{(m)}(\delta_1;0) \propto c + \sum_{l=1}^{N-1}(N-l)\cos(l\delta_1)$, with $\delta_j = \delta_j(\mathbf{r}_j) = kd\sin[\theta_j(\mathbf{r}_j)]$ [32,33]. Note that $g_N^{(m)}(\mathbf{r}_1)$ displays *all* $N-1$ different spatial frequencies ld, $l = 1, \ldots, N-1$, of the setup, equally obtained when measuring the intensity distribution of a coherently illuminated N slit grating with slit separation d.

For an irregular source arrangement with arbitrary separations it turns out that by placing $m-1$ detectors at the so-called *magic positions* [14]

$$\delta_j = 2\pi(j-2)/(m-1) \quad j = 2, \ldots, m, \tag{2}$$

all spatial frequencies of the source arrangement are suppressed in $g_N^{(m)}(\delta_1)$, except those fulfilling the condition

$$\kappa(m-1) = (x_{l_1} + \cdots + x_{l_2}) \in \{\xi\}, \tag{3}$$

with $\kappa \in \mathbb{N}$. In this case the mth-order intensity correlation function takes the form [21]

$$g_N^{(m)}(\delta_1) = A_0^{(m)} + \sum_\kappa A_\kappa^{(m)} \cos[\kappa(m-1)\delta_1], \tag{4}$$

where $A_\kappa^{(m)}$ is the amplitude of the modulation with frequency $\kappa(m-1)$; if no element of $\{\xi\}$ fulfills Eq. (3), i.e., all spatial frequencies $(x_{l_1} + \cdots + x_{l_2}) \in \{\xi\}$ differ from $\kappa(m-1)$, we obtain $g_N^{(m)}(\delta_1) = A_0^{(m)} = \text{const}$.

The magic positions can be determined by changing the positions $\mathbf{r}_2, \ldots, \mathbf{r}_m$ of the detectors $D_2, \ldots, D_m$ while monitoring the interference pattern $g_N^{(m)}(\delta_1)$ until a modulation of the form $\sum_\kappa A_\kappa^{(m)} \cos[\kappa(m-1)\delta_1]$ appears [34] (for details see Ref. [21]). In this case the relative phase relation $\delta_j - \delta_{j-1} = 2\pi/(m-1)$, $j = 3, \ldots, m$ is fulfilled [see Eq. (2)]. The lattice constant d can then be deduced from δ_j and δ_{j-1} via $d = \lambda/\{(m-1)[\sin(\theta_j) - \sin(\theta_{j-1})]\}$. Note further that, in view of Eqs. (3) and (4), the regular source distribution discussed in Ref. [14] is a special case of the outlined imaging protocol with $m = N$. Indeed, for $x_1 = x_2 = \cdots = x_{N-1} \equiv 1$ we obtain for $m = N$

$$g_N^{(N)}(\delta_1) = A_0^{(N)} + A_N^{(N)} \cos[(N-1)\delta_1]. \tag{5}$$

However, in contrast to Eq. (5), the spatial frequency filtering process of Eqs. (3) and (4) neither depends on the number of sources, i.e., it can be applied for $m \neq N$, nor does it rely on a particular source geometry $\mathbf{x}$ [21].

Measuring $g_N^{(m)}(\delta_1)$ for $m \geq 3$ allows us to determine all spatial frequencies $\in \{\xi\}$ fulfilling Eq. (3). However, since not all of the $N(N-1)/2$ spatial frequencies of the unknown source geometry $\mathbf{x}$ are necessarily different, the scheme has access only to the smaller set of all different spatial frequencies

$$\mathbf{F} \equiv \{\text{all different spatial frequencies} \in \{\xi\}\} = \{f_i\}. \tag{6}$$

$\mathbf{F}$ still contains a large amount of information, narrowing down the set of possible source geometries substantially so that in most cases a unique solution can be obtained.

Consider, for example, the case $\mathbf{x} = (3,1,4)$. Here, the set of different spatial frequencies is given by $\mathbf{F} = \{1,3,4,5,8\}$. Measuring all intensity correlation functions of order $3 \leq m \leq 9$ leads to a unique solution for the number and distribution of sources [21].

$$\mathbf{F} = \{1,3,4,5,8\} \rightarrow N = 4 \quad \text{with} \quad \mathbf{x} = (3,1,4); \tag{7}$$

i.e., a unique reconstruction (imaging) of the unknown source geometry can be achieved. By contrast, for the set of spatial frequencies $\mathbf{F} = \{1,3,4,5,8,9\}$ two possible solutions for the unknown source geometry exist, namely,

$$\mathbf{F} = \{1,3,4,5,8,9\} \rightarrow \begin{cases} N = 4 & \mathbf{x} = (1,3,5) \\ N = 5 & \mathbf{x} = (1,3,1,4). \end{cases} \tag{8}$$

To remove the remaining ambiguity, additional information can be extracted from the amplitudes $A_k^{(m)}$ of the correlation functions $g_N^{(m)}(\delta_1)$, $m \geq 3$ [cf. Eq. (4)]. As an example, we display $g^{(5)}(\delta_1)$ for the two scenarios of Eq. (8) in Fig. 2. The difference in (relative) amplitudes is clearly visible, enabling a discrimination between the two solutions. As it turns out a unique solution can always be obtained when using the information of the amplitudes of the correlation functions [21].

Note that the determination of $\mathbf{F}$ makes small demands to the experimental data as only the spatial frequencies are to be identified (see Fig. 3). The second step—reconstructing the source geometry $\mathbf{x}$ from $\mathbf{F}$—sometimes requires a better data quality as in order to remove ambiguities the amplitudes $A_k^{(m)}$ of the modulations have to be taken into account.

The proposed imaging technique allows us to reconstruct the source geometry $\mathbf{x}$ with a resolution below the Abbe limit. According to Abbe, for a given numerical aperture $\mathcal{A}$, the smallest resolvable distance is given by $d_{\min} = \lambda/(2\mathcal{A})$, where λ is the wavelength of the light emitted by the sources [35]. The range $\delta_1 \in [0, 2\pi]$ is required in the far field to resolve this distance as two adjacent principal maxima are separated by $\Delta\delta_1 = 2\pi$ [see dashed (black) arrow in Fig. 2(a)]. By contrast, using the imaging protocol outlined above, the moving detector D_1 requires only the range $\Delta\delta_1 = 2\pi/(m-1)$ to scan two adjacent maxima, as

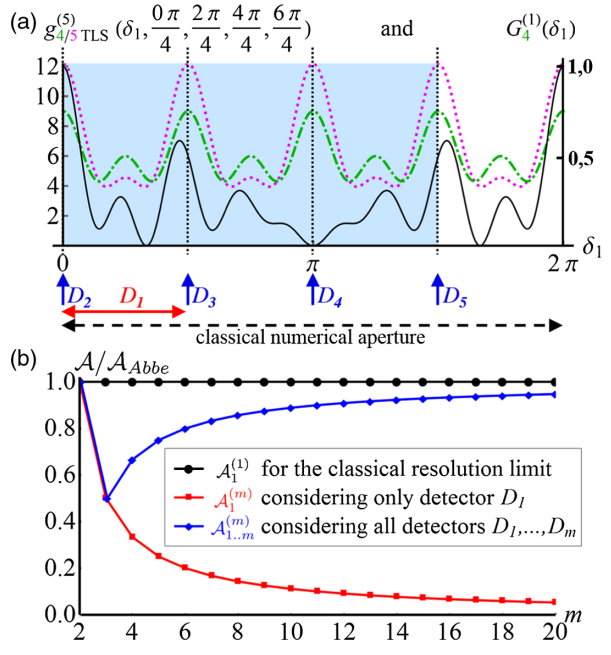

FIG. 2. (a) $G_N^{(1)}(\delta_1)$ for $N = 4$ coherently emitting sources with distances $\mathbf{x} = (3, 1, 4)$ [solid (black) curve] and $g_N^{(5)}(\delta_1)$ for both scenarios of Eq. (8): $N = 4$ TLS [dotted-dashed (green) curve] and $N = 5$ TLS [dotted (magenta) curve]; for the latter two cases four detectors are fixed at the magic positions. The numerical aperture $\mathcal{A}_1^{(1)}$ required by the classical Abbe limit is indicated by the dashed (black) arrow below the x axis; the numerical aperture $\mathcal{A}_1^{(m)}$ required for D_1 to scan from one to the next principal maxima is indicated by the solid (red) arrow below the x axis; the numerical aperture $\mathcal{A}_{1\ldots m}^{(m)}$ required by all detectors D_j, $j = 1, \ldots, 5$ is indicated by the blue-shaded area (see Fig. 1). (b) Numerical apertures $\mathcal{A}_1^{(1)}$, $\mathcal{A}_1^{(m)}$, and $\mathcal{A}_{1\ldots m}^{(m)}$ (in units of $\mathcal{A}_1^{(1)} = \mathcal{A}_{\mathrm{Abbe}}$) as a function of correlation order m. As can be seen, $\mathcal{A}_1^{(m)}$ and $\mathcal{A}_{1\ldots m}^{(m)}$ remain always smaller than $\mathcal{A}_1^{(1)}$.

the fringe spacing is reduced by $(m-1)$ [see Eq. (4)]. Because of the reduced numerical aperture $\mathcal{A}_1^{(m)}$ required for the moving detector, the resolution for the moving detector is enhanced by the same factor, i.e., overcoming the classical resolution limit by $(m-1)$ [see red squares in Fig. 2(b)] [14]. Considering the angular range of *all* detectors, i.e., including the detectors placed at the magic positions, the required numerical aperture $\mathcal{A}_{1\ldots m}^{(m)}$ increases [see blue diamonds in Fig. 2(b)]. However, $\mathcal{A}_{1\ldots m}^{(m)}$ remains below the aperture $\mathcal{A}_1^{(1)}$ required by the Abbe limit for all $m \geq 3$ [see Fig. 2(b)]. The proposed imaging protocol is thus able to reconstruct the source geometry with sub-classical resolution. Moreover, it allows us to determine the spatial frequencies of the source ensemble with a substantially reduced number of fit parameters in comparison to classical imaging techniques. In the former case only one or at most few spatial frequencies have to be determined from $g^{(m)}(\delta_1)$, whereas in the case of classical imaging techniques *all* spatial frequencies have to be identified in the Fourier plane at once.

For an experimental demonstration of the proposed imaging technique we used up to four statistically independent pseudothermal light sources (see Fig. 3). The pseudo-TLS were realized by use of a He-Ne laser at $\lambda = 632.8$ nm coupled into multimode fibers of diameter ~ 50 μm. The superposition of many modes in a given multimode fiber leads to a field with Gaussian statistics at the fiber output, equal to the Gaussian statistics of a TLS [36]. By mechanically shaking the fiber the modes are dynamically mixed leading to the required variation of the pseudothermal field in time. Since multiphoton interferences of classical sources can be measured in the high-intensity regime [37], a conventional digital camera located in the far field of the fibers ($z \approx 0.40$ m) was used to measure the light intensity. Each pixel of the camera can be regarded as an individual detector. Intensity correlations of arbitrary order $g^{(m)}(\delta_1, \ldots, \delta_m)$ can be derived by correlating the gray values of m pixels at δ_j, $j = 1, \ldots, m$ (see Fig. 1) [33]. A linear polarizer was placed in front of the camera to ensure that light of equal polarization is employed.

One-dimensional arrangements of pseudo-TLS with varying sets of source separations $\mathbf{x}$ were realized by placing the end facets of the fibers onto grooves of a mechanical grid with lattice constant $d = 570$ μm. In this way the source geometries displayed in Fig. 3 have been implemented. To obtain interference signals of high visibility, the integration time of the camera $\tau_i \sim 100$ μs was chosen to be much shorter than the coherence time of the TLS ($\tau_c \sim 10$ ms).

The experimental results for three different source arrangements are shown in Fig. 3. For each setup we collected $N = 1000$ camera images (corresponding to a total measurement time ~ 500 s), each with a different realization of the pseudothermal field. The intensity distribution was confirmed to be thermal by measuring the instantaneous intensities at each pixel over the set of 1000 camera images [36]. By correlating $m-1$ pixels at the magic positions [see Eq. (2)] with another pixel at δ_1 we derived $g^{(m)}(\delta_1)$ for $m = 3, \ldots, 6$. Note that the finite lateral extension of the pseudothermal sources should principally lead to a spatial envelope of $g^{(m)}(\delta_1)$. However, due to the small size of the fiber cores this modification is small and can be neglected (see Fig. 3); this allows us to use Eq. (4) as a fit function for the experimental results [21].

Table I displays the mean values for the set of spatial frequencies and corresponding amplitudes, obtained from a least squares fit for the correlation orders $m = 3, \ldots, 6$, together with their uncertainties, using ten different pixels for the phase reference $\delta_2 = 0$. According to the theory all occurring spatial frequencies should be integer numbers [see Eq. (3)]. This is confirmed to better than 5% by our

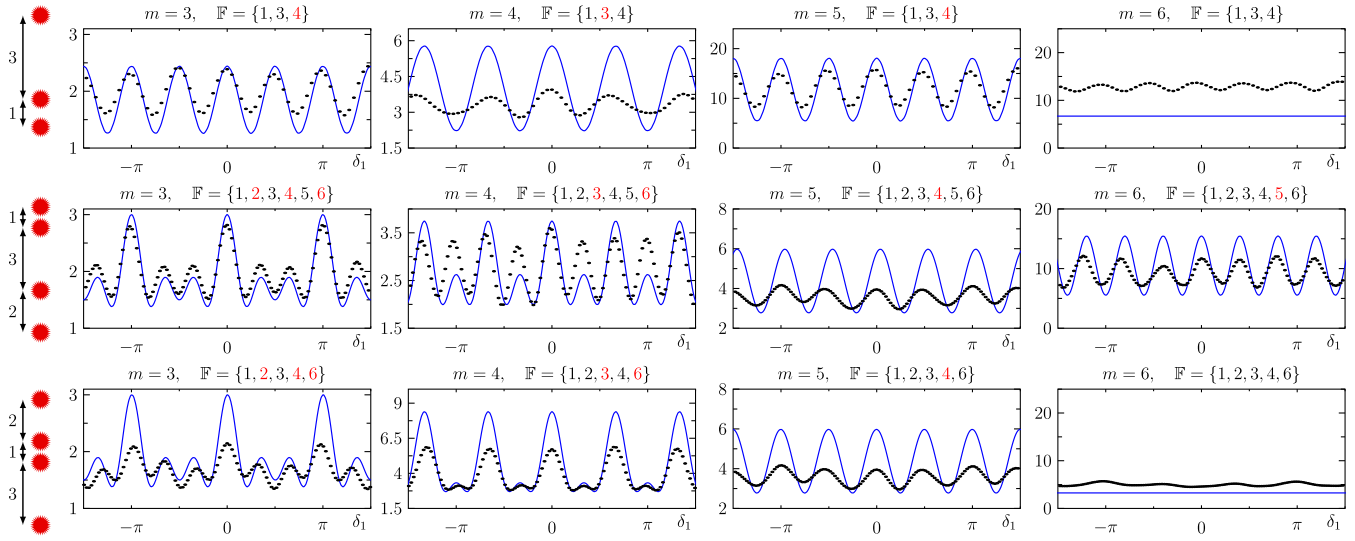

FIG. 3. Measured mth-order correlation function $g^{(m)}(\delta_1)$ for $m = 3, \ldots, 6$ [dotted (black) curves], where $m-1$ detectors are placed at the magic positions [see Eq. (2)], together with the theoretically expected signals according to Eq. (4) [solid (blue) curves] for the three source configurations shown on the left. The two lower configurations, having an equal set of source distances but different source arrangements $\mathbf{x}$ and thus different set of spatial frequencies $\mathbf{F}$, can be clearly distinguished by the imaging protocol.

experimental results, allowing us to uniquely identify the respective integers (see Table I). The measured amplitudes do not match the theory equally well as the spatial frequencies and show larger uncertainties (see Fig. 3 and Table I). Yet in all three cases the investigated source arrangements can readily be determined from the experimental data (see left side of Fig. 3).

The uncertainties consist of statistical errors (less than 1%) and systematic errors, e.g., due to the finite extensions of the sources, unequal intensities, and the finite size of the CCD pixels [21]. The latter prevents the $m-1$ fixed detectors from being located exactly at the magic positions. Hence, a modulation can be seen sometimes in the $g^{(m)}$ signal although a constant is expected. However, trying to fit these signals with a modulated function leads to extraordinarily large statistical errors of the fitted frequency, making these cases easily identifiable [see, e.g., $g_3^{(6)}(\delta_1)$ in Fig. 3 and Table I].

In conclusion, we presented a new imaging protocol making use of spatial intensity correlation functions $g^{(m)}$ of order $m \geq 3$ to derive the set of different spatial frequencies $\mathbf{F}$ of an arbitrary arrangement of TLS in one dimension. The scheme allows us to isolate the spatial frequencies of the system within different correlation orders; in this way all relevant information about the source distribution can be extracted with a substantially reduced number of fit parameters in comparison to classical imaging techniques. Linking $\mathbf{F}$ to the set of adjacent source distances $\mathbf{x}$ allows in most cases for a unique reconstruction, i.e., imaging, of the source arrangement; remaining ambiguities can be removed by taking the amplitudes of the modulations of $g^{(m)}$ into account. The scheme allows for subclassical imaging; i.e., it requires a numerical aperture smaller than the classical Abbe limit. Experimental results verifying the theoretical predictions are presented. The method relies on linear optical detection and spatial photon cross correlations in

TABLE I. Experimentally measured mean values for the spatial frequencies f_i and corresponding amplitudes $A_i^{(m)}$ according to Eqs. (3) and (4), obtained for the correlation orders $m = 3, \ldots, 6$, with corresponding uncertainties (for details see text).

		$\mathbf{m=3}$		$\mathbf{m=4}$		$\mathbf{m=5}$		$\mathbf{m=6}$	
x	**F**	$\overline{f_i}$	$\overline{A_i^{(3)}}$	$\overline{f_i}$	$\overline{A_i^{(4)}}$	$\overline{f_i}$	$\overline{A_i^{(5)}}$	$\overline{f_i}$	$\overline{A_i^{(6)}}$
(3, 1)	$\{1,3,4\}$	4.02 ± 0.10	0.32 ± 0.08	2.93 ± 0.10	0.51 ± 0.19	4.02 ± 0.10	2.47 ± 0.88	3.90 ± 0.40	1.05 ± 0.66
		1.96 ± 0.06	0.20 ± 0.04	3.02 ± 0.09	0.08 ± 0.01	3.98 ± 0.10	1.09 ± 0.24	4.93 ± 0.13	1.28 ± 0.16
(1, 3, 2)	$\{1,2,3,4,5,6\}$	3.98 ± 0.10	0.25 ± 0.03	5.94 ± 0.15	0.59 ± 0.15				
		5.94 ± 0.15	0.33 ± 0.05						
		2.09 ± 0.06	0.18 ± 0.02	3.01 ± 0.08	1.29 ± 0.14	4.00 ± 0.10	0.56 ± 0.13	2.99 ± 0.62	0.58 ± 0.52
(2, 1, 3)	$\{1,2,3,4,6\}$	3.97 ± 0.10	0.05 ± 0.01	6.06 ± 0.15	0.51 ± 0.08				
		6.06 ± 0.15	0.17 ± 0.03						

the far field of the sources. It thus differs from super-resolving multiphoton imaging techniques based on nonlinear effects in particular atomic transitions [38–40], or exploiting higher order autocorrelations [15–17,19]. As this approach is independent from the photon wavelength and works without refractive optical elements, potential applications in x-ray imaging but also in astronomy, biology, medicine, and the technical sciences are expected, potentially limited to smaller numbers of sources.

The authors gratefully acknowledge funding by the Erlangen Graduate School in Advanced Optical Technologies (SAOT) by the German Research Foundation (DFG) in the framework of the German excellence initiative. D. B. gratefully acknowledges financial support by the Cusanuswerk, Bischöfliche Studienförderung. J. v. Z and A. C gratefully acknowledge financial support by the Staedtler Stiftung.

*Corresponding author.
anton.classen@fau.de

[1] D. Leibfried, M. D. Barrett, T. Schaetz, J. Britton, J. Chiaverini, W. M. Itano, J. D. Jost, C. Langer, and D. J. Wineland, Science **304**, 1476 (2004).
[2] A. N. Boto, P. Kok, D. S. Abrams, S. L. Braunstein, C. P. Williams, and J. P. Dowling, Phys. Rev. Lett. **85**, 2733 (2000).
[3] M. D'Angelo, M. V. Chekhova, and Y. Shih, Phys. Rev. Lett. **87**, 013602 (2001).
[4] M. W. Mitchell, J. S. Lundeen, and A. M. Steinberg, Nature (London) **429**, 161 (2004).
[5] P. Walther, J.-W. Pan, M. Aspelmeyer, R. Ursin, S. Gasparoni, and A. Zeilinger, Nature (London) **429**, 158 (2004).
[6] P. R. Hemmer, A. Muthukrishnan, M. O. Scully, and M. S. Zubairy, Phys. Rev. Lett. **96**, 163603 (2006).
[7] M. C. Teich and B. E. A. Saleh, Cesk. Cas. Fyz. **47**, 3 (1997).
[8] A. Muthukrishnan, M. O. Scully, and M. S. Zubairy, J. Opt. B: Quantum Semiclass. Opt. **6**, S575 (2004).
[9] G. S. Agarwal, G. O. Ariunbold, J. von Zanthier, and H. Walther, Phys. Rev. A **70**, 063816 (2004).
[10] C. Thiel, T. Bastin, J. Martin, E. Solano, J. von Zanthier, and G. S. Agarwal, Phys. Rev. Lett. **99**, 133603 (2007).
[11] S.-H. Tan, B. I. Erkmen, V. Giovannetti, S. Guha, S. Lloyd, L. Maccone, S. Pirandola, and J. H. Shapiro, Phys. Rev. Lett. **101**, 253601 (2008).
[12] S. Lloyd, Science **321**, 1463 (2008).
[13] V. Giovannetti, S. Lloyd, L. Maccone, and J. H. Shapiro, Phys. Rev. A **79**, 013827 (2009).
[14] S. Oppel, T. Büttner, P. Kok, and J. von Zanthier, Phys. Rev. Lett. **109**, 233603 (2012).
[15] O. Schwartz and D. Oron, Phys. Rev. A **85**, 033812 (2012).
[16] O. Schwartz, J. M. Levitt, R. Tenne, S. Itzhakov, Z. Deutsch, and D. Oron, Nano Lett. **13**, 5832 (2013).
[17] T. Dertinger, A. Pallaoro, G. Braun, S. Ly, T. A. Laurence, and S. Weiss, Q. Rev. Biophys. **46**, 210 (2013).
[18] E. D. Lopaeva, I. Ruo Berchera, I. P. Degiovanni, S. Olivares, G. Brida, and M. Genovese, Phys. Rev. Lett. **110**, 153603 (2013).
[19] D. Gatto Monticone, K. Katamadze, P. Traina, E. Moreva, J. Forneris, I. Ruo-Berchera, P. Olivero, I. P. Degiovanni, G. Brida, and M. Genovese, Phys. Rev. Lett. **113**, 143602 (2014).
[20] M. E. Pearce, T. Mehringer, J. von Zanthier, and P. Kok, Phys. Rev. A **92**, 043831 (2015).
[21] See Supplemental Material at http://link.aps.org/supplemental/10.1103/PhysRevLett.117.253601 for more detailed descriptions and calculations, which includes Refs. [22–30].
[22] I. S. Reed, IRE Trans. Inf. Theory **8**, 194 (1962).
[23] P. van Cittert, Physica (Amsterdam) **1**, 201 (1934).
[24] F. Zernike, Physica (Amsterdam) **5**, 785 (1938).
[25] H. J. Ryser, *Combinatorial Mathematics*, Carus Mathematical Monographs (Mathematical Association of America, Wiley, New York, 1963).
[26] D. G. Glynn, Eur. J. Combinatorics **31**, 1887 (2010).
[27] D. Zhang, Y.-H. Zhai, L.-A. Wu, and X.-H. Chen, Opt. Lett. **30**, 2354 (2005).
[28] X.-H. Chen, Q. Liu, K.-H. Luo, and L.-A. Wu, Opt. Lett. **34**, 695 (2009).
[29] P. K. Tan, G. H. Yeo, H. S. Poh, A. H. Chan, and C. Kurtsiefer, Astrophys. J. Lett. **789**, L10 (2014).
[30] R. Hanbury Brown and R. Q. Twiss, Nature (London) **178**, 1046 (1956).
[31] R. J. Glauber, Phys. Rev. **130**, 2529 (1963).
[32] D. Bhatti, S. Oppel, R. Wiegner, G. S. Agarwal, and J. von Zanthier, Phys. Rev. A **94**, 013810 (2016).
[33] S. Oppel, R. Wiegner, G. S. Agarwal, and J. von Zanthier, Phys. Rev. Lett. **113**, 263606 (2014).
[34] If no modulation appears in $g_N^{(m)}(\delta_1)$ this means that the setup contains no spatial frequency fulfilling the condition of Eq. (3).
[35] M. Born and E. Wolf, *Principles of Optics*, 7th ed. (Cambridge University Press, Cambridge, 1999).
[36] T. Mehringer, S. Oppel, and J. von Zanthier, arXiv:1611.09161.
[37] I. N. Agafonov, M. V. Chekhova, T. S. Iskhakov, and A. N. Penin, Phys. Rev. A **77**, 053801 (2008).
[38] S. W. Hell and J. Wichmann, Opt. Lett. **19**, 780 (1994).
[39] E. Betzig, Opt. Lett. **20**, 237 (1995).
[40] R. M. Dickson, A. B. Cubitt, R. Y. Tsien, and W. E. Moerner, Nature (London) **388**, 355 (1997).